https://doi.org/10.5194/wes-2021-12
Preprint. Discussion started: 5 March 2021

eawe european academy of wind energy
Open Access WIND ENERGY SCIENCE DISCUSSIONS

UNAFLOW: a holistic experiment about the aerodynamics of floating wind turbines under imposed surge motion

Alessandro Fontanella[1], Ilmas Bayati[2], Robert Mikkelsen[3], Marco Belloli[1], and Alberto Zasso[1]

[1]Mechanical Engineering Department, Politecnico di Milano, Milano, Via La Masa 1, 20156, Italy.
[2]Maritime Research Institute Netherlands (MARIN), Wageningen, 6708 PM, The Netherlands.
[3]Technical University of Denmark (DTU), Department of Wind Energy, Lyngby, Denmark.

Correspondence: Alessandro Fontanella (alessandro.fontanella@polimi.it)

Abstract. Floating offshore wind turbines are subjected to large motions because of the additional degrees of freedom offered by the floating foundation. The rotor operates in highly dynamic inflow conditions and this is deemed to have a significant effect on the aerodynamic loads, as well as on the wind turbine wake. Floating wind turbines and floating farms are designed by means of numerical tools, that have to model these unsteady aerodynamic phenomena to be predictive of reality. Experiments are needed to get a deeper understanding of the unsteady aerodynamics, and hence leverage this knowledge to develop better models, as well as to produce data for the validation and calibration of the existing tools. This paper presents a wind-tunnel scale-model experiment about the unsteady aerodynamics of floating wind turbines that followed a radically different approach than the other existing experiments. The experiment covered any aspect of the problem in a coherent and structured manner, that allowed to produce a low-uncertainty data for the validation of numerical model. The data covers the unsteady aerodynamics of the floating wind turbine in terms of blade forces, rotor forces and wake. 2D sectional model tests were carried to study the aerodynamics of a low-Reynolds blade profile subjected to a harmonic variation of the angle of attack. The lift coefficient shows an hysteresis cycle that extends in the linear region and grows in strength for higher motion frequencies. The knowledge gained in 2D sectional model tests was exploited to design the rotor of a 1/75 scale model of the DTU 10MW that was used to perform imposed surge motion tests in a wind tunnel. The tower-top forces were measured for several combinations of mean wind speed, surge amplitude and frequency to assess the effect of unsteady aerodynamics on the response of the system. The thrust force, that plays a crucial role in the along-wind dynamics of a floating wind turbine mostly follows the quasi-steady theory. The near-wake of the wind turbine was studied by means of hot-wire measurements, and PIV was utilized to visualize the tip vortex. It is seen that the wake energy is increased in correspondence of the motion frequency and this is likely to be associated with the blade-tip vortex, which travel speed is modified in presence of surge motion.

1 Introduction

Floating offshore wind is receiving a growing interest as it makes it possible to harvest the wind energy resource of deep waters, which cannot be exploited a cost competitive price with conventional bottom-fixed wind turbines. Floating offshore wind turbines (FOWTs) are subjected to large and low-frequency motions that are the cause of unsteady aerodynamics effects. The rotor of an FOWT operates in dynamic inflow conditions de Vaal et al. (2014), mainly for two reasons: the platform motion

https://doi.org/10.5194/wes-2021-12
Preprint. Discussion started: 5 March 2021

eawe european academy of wind energy
Open Access WIND ENERGY SCIENCE DISCUSSIONS

modifies the wind speed seen by the rotor, and moves the rotor in its own wake. This has a significant effect on the aerodynamic loads and, consequently, on the response of the FOWT. Moreover, the platform motions result into large-scale motions of the wind turbine wake, which are relevant for the wake-interaction in floating farms Wise and Bachynski (2020).

Wind turbines and wind farms are designed and studied by means of numerical simulation tools, that are in large part developed for bottom-fixed wind turbines. Experiments are needed to assess wether these models are predictive also for wind turbines with a floating foundation, to get a deeper understanding of the peculiar aerodynamic phenomena that occurs when the wind turbine undergoes large motions and, based on this knowledge, to develop better simulations tools. Even though the importance of the aerodynamics of FOWTs is widely recognized, few are the experiments that tried to shed light into this topic. In R. Farrugia and T. Sant and D. Micallef (2014) wave-basin tests were carried out about a TLP-FOWT subjected to regular waves, measuring the wind turbine power and wake. In Hu et al. (2015), a 1/300 Froude-scaled wind turbine model was installed on a 3-DOF motion simulator in a wind tunnel. PIV was used to obtain a flow description in the near wake region (x/D$<$2) and structural loads where measured when the system was subjected to surge motion. In Shifeng Fu and Yaqing Jin and Yuan Zheng and Leonardo P. Chamorro (2019), wind tunnel experiments were performed to assess the effect of pitch and roll oscillations on power output and wake of a wind turbine scale model (12cm rotor diameter). The experiment did not consider the rotor thrust force, that is strongly coupled with the platform motions. In Schliffke et al. (2020) a porous disk model is used to represent a 2MW FOWT at 1/500 scale, and study its wake at a distance of 4.6D when subjected to an imposed surge motion. The porous disk concept has some inherent limitations: it is not valid to study the near wake and does not reproduce the local aerodynamic loads of the blades. In the wind tunnel tests of Bayati et al. (2016) a high-fidelity 1/75 scale model of the DTU 10MW wind turbine is used to study the effect of imposed surge and pitch motion on the rotor thrust force. Measurements are compared to FAST simulations to assess the prediction capabilities of AeroDyn with respect to FOWTs. Numerical and experimental results showed some discrepancies that suggested the need to study the problem further. In Bayati et al. (2017b), a second test campaign is carried out to study by means hot-wire measurements the near-wake of the same scale model under imposed surge motion.

The UNAFLOW experiment was built on the experience gained in Bayati et al. (2016, 2017b). The aim of the project was to study the unsteady aerodynamics of FOWTs following a holistic and systematic approach. The experiment generated a comprehensive database, that covers the unsteady aerodynamics of the wind turbine blade, the rotor forces and the near wake. Because of these aspects, the experiment can be considered as the most advanced wind tunnel test on the topic of unsteady FOWT aerodynamics to date. Thanks to the systematic approach, the experimental data are featured by a low uncertainty level, that promotes their use as a benchmark for the development of numerical tools. In Cormier et al. (2018), measurements were compared to a BEM, free-vortex and fully-resolved CFD model. A second comparison withnumerical models was recently carried out in Mancini et al. (2020) concerning the rotor thrust and power. The full dataset of the UNAFLOW experiments is freely available for the community for further studies.

The aim of this paper is to twofold. First it presents the experiment, the methodology it was followed to design it, and that was used to carry out measurements later. Second, it presents the available dataset, serving as an accompaniment to them, and summarizes the most significant results from the experiment. The structure of the remainder of the paper is as follows. Section

https://doi.org/10.5194/wes-2021-12
Preprint. Discussion started: 5 March 2021

2 describes the approach that was followed to design the experiment, and to select the tested conditions. Section 3 presents the 2D sectional model tests that were carried out at the Technical University of Denmark (DTU) Red wind tunnel, to characterize the aerodynamic coefficients of the SD7032 airfoil, used in the scale model turbine blades. Section 4 describes the full-turbine experiment, with emphasis on the wind turbine scale model and the measurements that were carried out. Section 5 reports the main findings of the full-turbine experiments with surge motion, in particular those about the rotor thrust force, the energy content of the near-wake, and the tip-vortex structure. Section 6 draws the conclusions and gives some recommendations for future research.

2 Concept and design of the experiment

The rotor of an FOWT is often working in strong unsteady conditions, because of the large rigid-body motions that arise because the low-compliance of the floating platform and wave excitation. The UNAFLOW projects studied the unsteady behavior of an FOWT rotor, and the core of the experimental activity was an extensive wind tunnel test campaign with a high-fidelity wind turbine scale model subjected to imposed surge motion. The wind turbine was a 1/75 model of the DTU 10MW Bak et al. (2013), with a 2.38m diameter rotor designed to match the thrust and power coefficient of the reference wind turbine. The purpose of the wind tunnel experiment was tp provide a large dataset of rotor integral loads and wake measurements for several wind-turbine operating and motion conditions, selected to be realistic for a multi-megawatt FOWT. 2D sectional airfoil experiments were carried out prior to the full-turbine tests, to guide the selection of the motion conditions for the turbine scale model, and to support the creation of numerical models of the experiment.

2.1 Wind conditions

The experiment considered three operating conditions which are reported in table 1. No closed-loop control strategy is utilized, and the rotor speed and the collective pitch angles were fixed. In the first two conditions, the wind turbine is operated at the optimum value of tip-speed ratio (TSR) and power is extracted with maximum efficiency (i.e. the maximum power coefficient is achieved). Being the TSR the same, the angle of attack (AoA) along the blade is the same in the RATED1 and RATED2 conditions. In the second condition, the TSR is lower and the collective pitch angle is increase, to get a lower power coefficient. Experiments were carried out in smooth flow conditions, and the turbulence index across the test section height was approximately 2%.

Table 1. Tested wind turbine operating conditions (RS is the rotor speed, CP is the rotor collective pitch angle).

Condition	V [m/s]	RS [rpm]	TSR [-]	CP [deg]
RATED1	2.5	150	7.5	0
RATED2	4.0	241	7.5	0
ABOVE	6.0	265	5.5	12.5

https://doi.org/10.5194/wes-2021-12
Preprint. Discussion started: 5 March 2021

eawe european academy of wind energy
Open Access WIND ENERGY SCIENCE DISCUSSIONS

Figure 1 shows the Reynolds number along the span of the wind-turbine scale-model blade in the three operating conditions of Table 1. The Reynolds number is over 80k for most of the blade span in RATED2 and ABOVE conditions, and it drops to 50k in RATED1 wind speed. 2D airfoil sectional model experiments were carried out to measure the aerodynamic coefficients of the blade airfoil for a range of Reynolds number close to those experience by the blade in full-turbine tests.

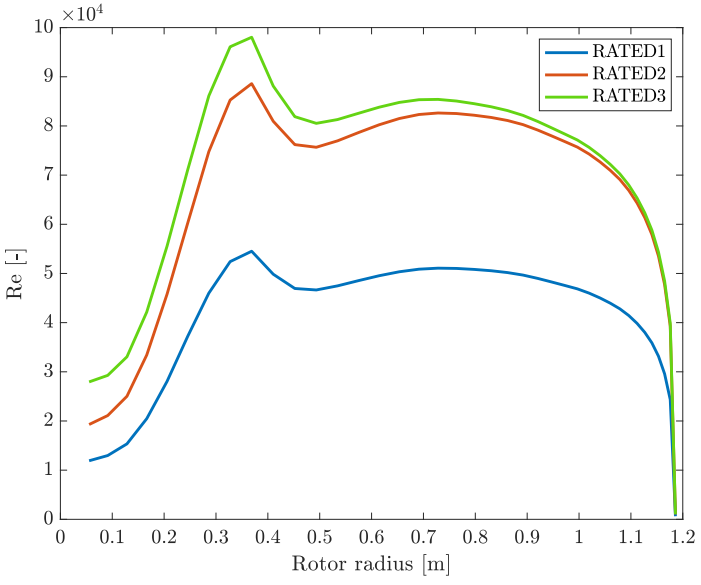

Figure 1. Reynolds number along the span of the wind-turbine scale-model blade in the three operating conditions of the experiment.

2.2 Motion conditions

The aim of the experiment was to investigate the unsteady aerodynamics of an FOWT rotor associated with the rigid-body motion of the support platform. The unsteady aerodynamic problem is a complex multi-physics subject: the platform motion is driven by the wave excitation and depends on the characteristics of the platform itself. To keep the focus on the aerodynamic problem, some simplifying assumptions were made for what concerns the wave simulation and the resulting motion. The wind turbine model was forced to move in the surge direction and the other platform motions were not considered. The surge motion was selected because it produces an along-wind motion of the wind turbine, which is in turn cause of a large variation of the wind speed seen by the rotor. Moreover, in the surge motion, any point of the wind turbine rotor moves with the same velocity. This simplifies the modeling of the aerodynamics as the effective wind speed is uniform across the rotor.

The surge motion x considered in the experiments is mono-harmonic:

$$x = A_s \sin(2\pi f_s t)\,, \tag{1}$$

https://doi.org/10.5194/wes-2021-12
Preprint. Discussion started: 5 March 2021

eawe european academy of wind energy
Open Access WIND ENERGY SCIENCE DISCUSSIONS

where A_s and f_s are the amplitude and frequency of motion respectively. The experiment investigated several mono-harmonic motions, obtained from the combination of different values of amplitude and frequency.

Seven frequencies were selected in the range [0.125 - 2] Hz (model scale) which corresponds to the low-frequency range for semi-sub and spar platforms. Large motions are expected in this range of frequencies, as the rigid-body motion modes are excited in resonance. The maximum frequency investigated in the full-turbine experiment was limited to 2 Hz to avoid exciting the first tower fore-aft flexible mode. The effect the frequency of motion has on the rotor aerodynamics is qualitatively described by the wake reduced-velocity parameter introduced in Bay (2017):

$$V_w^* = \frac{V}{f_s D}\,, \tag{2}$$

where D is the rotor diameter, which is adopted as reference length, since it is widely used to describe the wake interaction in wind turbines. A high V_w^* means the air particles flow across the wind turbine in a short time, its path is not influenced by the wind turbine motion and the flow is quasi-steady. The lower the wake reduced velocity, the higher the unsteady effects.

Four amplitudes were tested for each combination of frequency and mean wind speed V. The selection of the values of amplitude was based on the maximum surge velocity:

$$\max(\dot{x}) = \Delta V = 2\pi f_s A_s\,. \tag{3}$$

The surge motion causes a variation of the angle of attack along the blades that is, in first approximation, proportional to:

$$\Delta V^* = \frac{\Delta V}{V}\,. \tag{4}$$

The four amplitude values were initially selected to achieve, for any pairing of wind speed and motion frequency, $\Delta V^* = 1/20, 3/80, 1/40, 1/80$. At low frequencies, the desired amplitude of motion was bigger than the stroke of the hydraulic actuator and it was reduced in reason of this constraint. Moreover, the amplitudes of the 1 Hz-frequency cases were increased by 50% to investigate a larger range of ΔV^*.

Figure 2 reports the average AoA along the blade span in the operating conditions of Table 1 and the maximum variation caused by the unsteady inflow associated with harmonic surge motion. Most of the blade sections work far from the stall front, and the surge motion causes a variation of the AoA of some degrees. An additional set of 2D sectional model tests was carried out to characterize the unsteady aerodynamic behavior of the blade airfoil for a harmonic variation of the AoA. The amplitude and frequency of the latter covered the AoA variation experience by the full-turbine blades because of the surge motion.

3 The 2D experiments

2D sectional-model experiments were conducted at the DTU Red wind tunnel to characterize the SD7032 profile behavior in steady and unsteady conditions. Steady experiments, with fixed AoA provided the airfoil polars for the range of Reynolds numbers that is of interest for the blade of the wind turbine scale model. The experimental polars were used to support the design of the scale model rotor, and to define the conditions of the full-turbine experiment. Polars were also used for the

https://doi.org/10.5194/wes-2021-12
Preprint. Discussion started: 5 March 2021

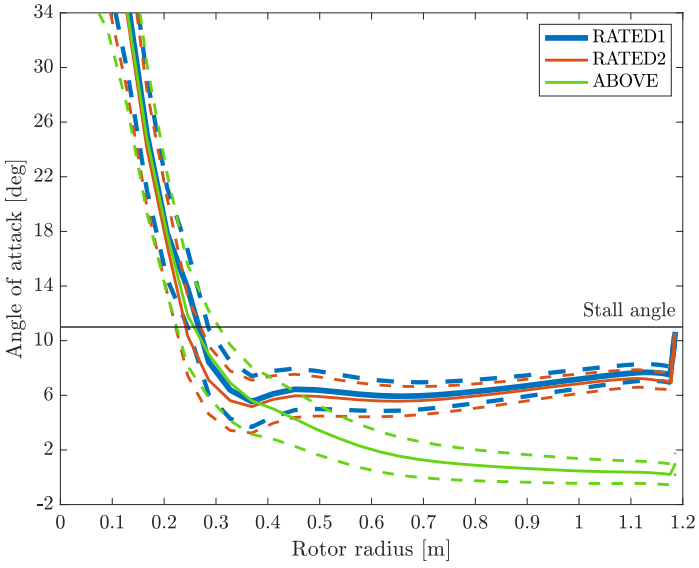

Figure 2. Average (solid lines) angle of attack along the span of the wind-turbine scale-model blade in the three operating conditions. The dashed lines in the corresponding colors show the maximum variation of the angle of attack because of the imposed surge motion.

calibration of numerical models of the experiment Cormier et al. (2018); Mancini et al. (2020). Unsteady experiments, with harmonic variation of the AoA, gave an insight into the unsteady aerodynamics of the airfoil. Results were used to support the design of the 3D experiment. In the UNAFLOW project there was not a specific effort to reproduce numerically the unsteady airfoil behavior, however, a wide dataset of unsteady polars are provided as project output. This data could be used both to validate unsteady airfoil aerodynamic models Boorsma and Caboni (2020) or unsteady CFD computation aiming to catch lift and drag oscillation due to dynamic variation of AoA.

The setup for 2D experiments is depicted in Figure 3. The 2D wing model, of 130mm chord, was fitted with a pressure loop (with 32 taps) at midspan that was used to measure the lift force from the pressure distribution, and a single-component force transducer that provided an additional lift force gage. The profile drag was obtained by means of a down-stream wake rake. The profile was mounted on a turning table that set the angle of attack.

3.1 Steady force coefficients

The force coefficients were measured for chord Reynolds number equal 50k, 60k, 75k, 100k, 150k, 200k and stepping through the AoA range from -10° to 25°. The Reynolds range covers the flow condition experienced by the blade of the wind turbine scale model (see Figure 1). Measurements were repeated in smooth flow (turbulence intensity lower than 0.1%), and with an increased free-stream turbulence that was obtained placing three thin wires (0.15mm diameter) about four chords upstream the profile. The slight increase in turbulence intensity, avoids the formation of a laminar separation bubble by tripping the boundary

https://doi.org/10.5194/wes-2021-12
Preprint. Discussion started: 5 March 2021

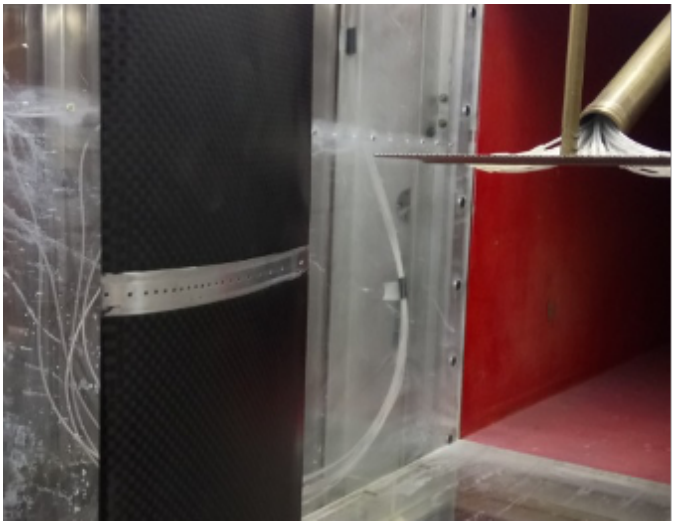

Figure 3. The experimental setup that was used to measure the blade polars in the DTU Red wind tunnel. The pressure loop is at the midspan of the blade sectional model, and the wake-rake is visible downstream.

layer. This inflow condition is deemed to be more realistic and closer to what is experienced by the wind turbine scale model. The lift and drag force coefficients are shown in Figure 4. The lift coefficient shows a non-linear behavior in correspondence of the stall AoA, which is clearly present at Re 50k, and becomes less evident for increasing Re values. The increased turbulence results in a smoother drag coefficient for any Re value. The effect on the lift coefficient is to smear out the non-linearity, and this is specially evident for Re values lower than 100k.

3.2 Unsteady force coefficients

The lift and drag force coefficient were also measured with an unsteady pitching of the airfoil. The conditions of the 2D experiment reflected those of the full-turbine blade. The experiments investigated the profile behavior for chord-Reynolds number of 50k, 100k, 150k, and a static AoA of 0, 3, 6, 9, 10, 12, 15 degrees. The amplitude and frequency of the sinusoidal pitching reflects the AoA variation produced by the imposed surge motion in the wind turbine scale model. The AoA amplitude was 0.5, 1, 2, 5 and the frequency of 0.25, 0.5, 1, 2, 3 Hz.

An example of the results is reported in Figure 5, with reference to the inflow with increased turbulence, a chord Re of 50k, and a sinusoidal variation of the AoA of 5 degrees amplitude and different frequencies. An hysteresis cycle is always present when the airfoil is pitched in correspondence of the stall AoA, and increasing the motion frequency, the strength of this effect is increased. The amplitude of the hysteresis cycle is instead small in the linear region (i.e. for AoA lower than the stall value), where most of the wind turbine model blade operates (see Figure 2).

https://doi.org/10.5194/wes-2021-12
Preprint. Discussion started: 5 March 2021

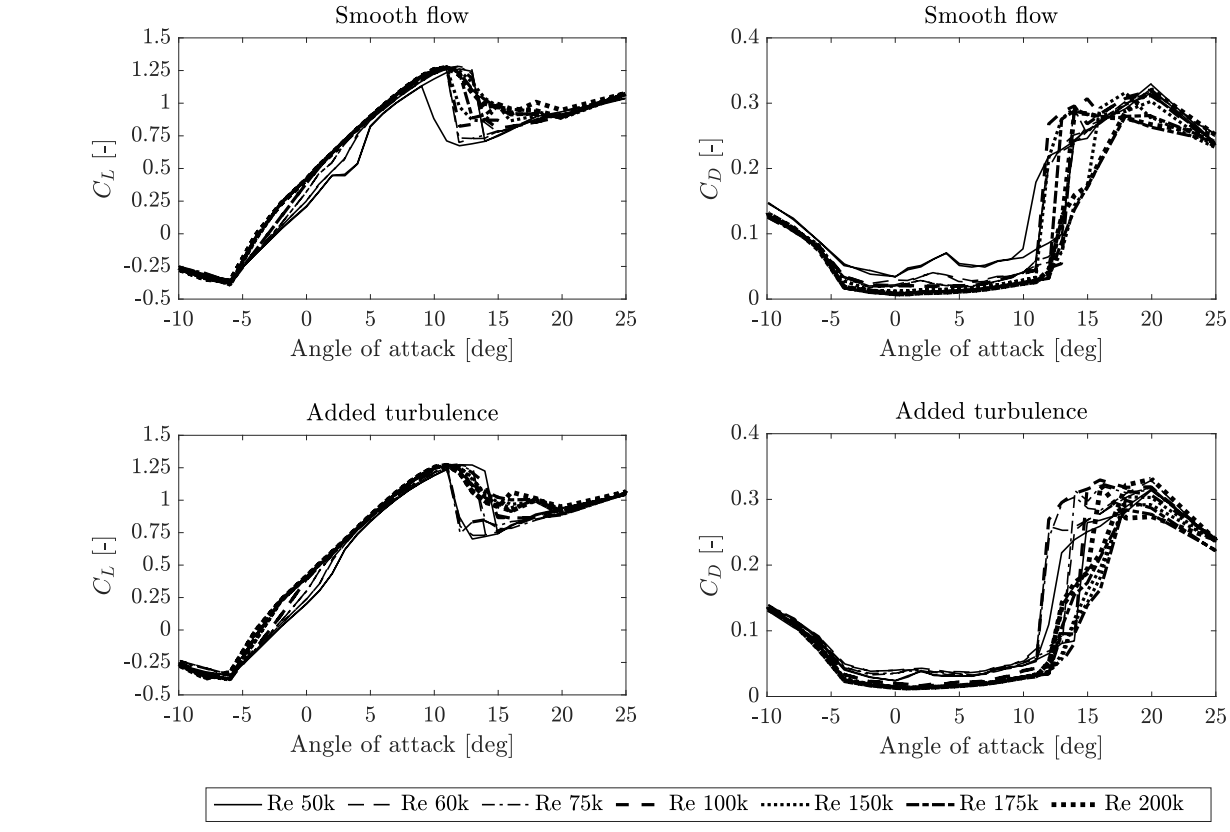

Figure 4. Steady lift (C_L) and drag (C_D) coefficients from 2D sectional model tests in smooth flow (top) and with added turbulence (bottom).

4 The full-turbine experiments

The UNAFLOW experiments were carried out at the Politecnico di Milano wind tunnel (Galleria del Vento Politecnico di Milano, GVPM GVP (2019)). The facility is a closed-loop subsonic wind tunnel and the flow is generated by 14 fans. UNAFLOW tests were carried out in the low-speed test chamber, which has a cross section of 3.84x13.84 m.

The wind turbine scale model was mounted on the test rig shown in Figure 6. The test rig is formed by a slider which is driven by a first hydraulic actuator, and is utilized to simulate the surge motion. On top of the slider, there is a second hydraulic actuator which is connected to the base of the wind turbine tower through a slider-crank mechanism. The second actuator was utilized to tilt the wind turbine so to have the rotor plane normal to the ground. In this way, the periodic effects due to the rotor tilt angle were avoided.

The experiment investigated three wind turbine operating conditions and several types of surge motion. The tested conditions are reported in Tables A1-A3, while the rationale behind their selection is explained in the rest of this section.

https://doi.org/10.5194/wes-2021-12
Preprint. Discussion started: 5 March 2021

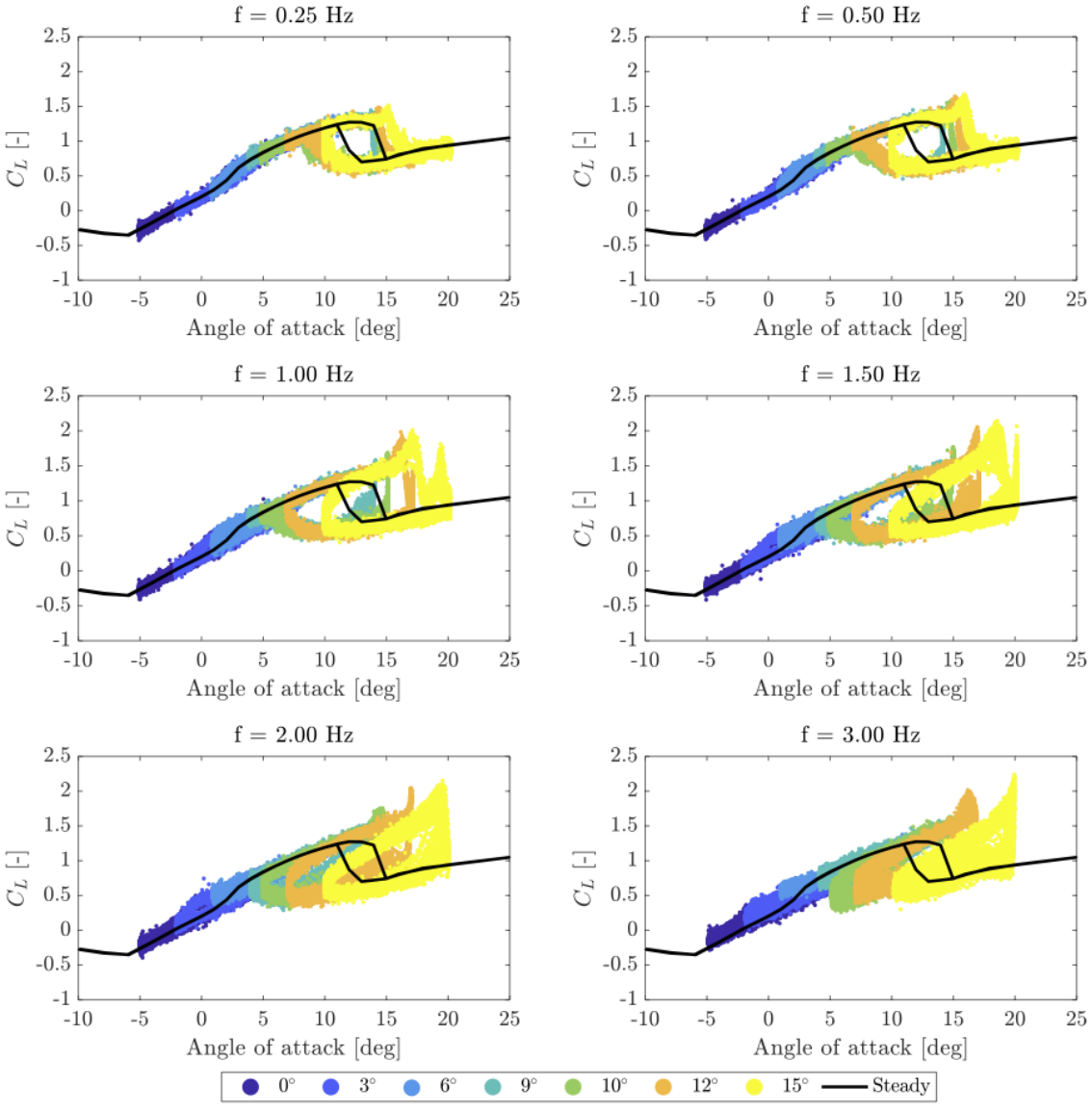

Figure 5. Unsteady lift coefficient (C_L) for a sinusoidal angle of attack variation of 5° and different frequencies, with increased inflow turbulence and a chord Re of 50k. The color of the dots denotes the mean angle of attack, and the steady lift coefficient is reported in black.

4.1 The wind turbine scale model

The wind turbine is a 1/75 scale model of the DTU 10MW Bak et al. (2013), that was designed within the LIFES50+ EU H2020 project Bayati et al. (2017). The rotor was designed based on the performance-scaling approach Kim (2014) to correctly

https://doi.org/10.5194/wes-2021-12
Preprint. Discussion started: 5 March 2021

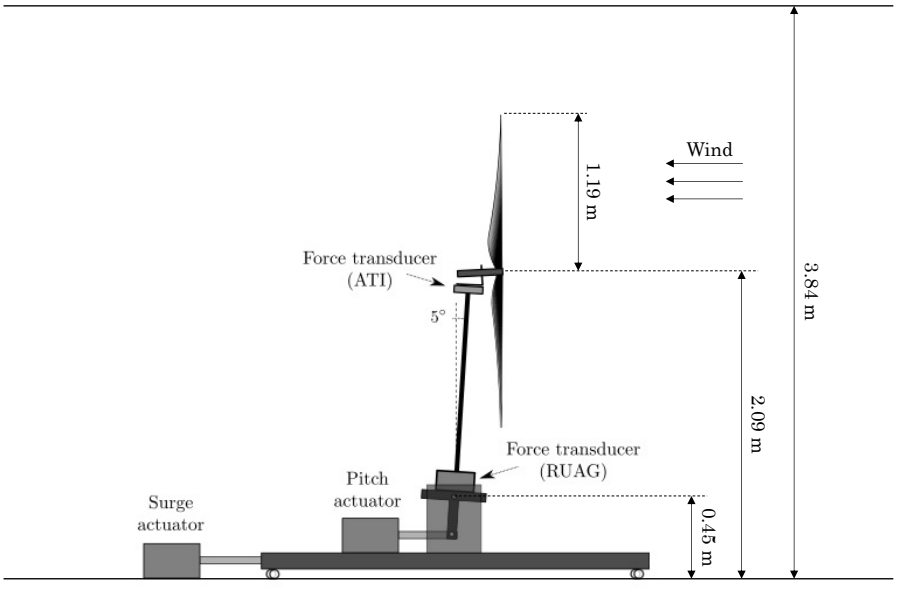

Figure 6. Schematic of the wind tunnel test setup, of the wind turbine scale model geometry, and the force transducers.

reproduce the thrust force coefficient of the full-scale reference wind turbine Bayati et al. (2017a). The scale model specification are reported in Table 2.

Table 2. Specifications of the wind turbine scale model (RNA stands for rotor-nacelle aseembly).

Parameter	Unit	Value
Rated wind speed	m/s	3.80
Rated rotor speed	rpm	240
Rotor diameter	m	2.38
Blade length	m	1.10
Hub diameter	m	0.18
Shaft tilt angle	deg	5.00
Blade mass	kg	0.21
Nacelle mass	kg	1.79
RNA mass	kg	3.58

https://doi.org/10.5194/wes-2021-12
Preprint. Discussion started: 5 March 2021

eawe european academy of wind energy
Open Access WIND ENERGY SCIENCE DISCUSSIONS

4.2 Measurements

Several measurements were carried out during the experiments. The undisturbed wind velocity V was measured by a Pitot tube that was located 5 m upstream the wind turbine, at 1.5 m height from the floor. An LVDT sensor provided the feedback for the control system of the surge hydraulic actuator. In parallel, the wind turbine surge motion was measured by means of a MEL M5L/200 laser sensor. The tower-top forces were measured by a 6-components force transducer. Two PCB MEMS accelerometers were fixed in correspondence of the tower-base to measured the x and z acceleration; another two were mounted on the nacelle to measure the x and y acceleration. All instruments were sampled synchronously with a frequency of 2000 Hz. In few selected test cases, the wake of the wind turbine was scanned by tri-axial hot-wire probes. In an even smaller sample of test cases, PIV measurements were carried out to describe the wake flow structure.

4.3 Tower-top forces

The six-components constraint force at the tower-top was measured by an ATI Mini45 SI-145-5 force transducer. Such measurements cannot be used directly to evaluate the aerodynamic forces because they also include the rotor-nacelle assembly (RNA) weight and inertia. To isolate the aerodynamic fraction of the force measurement, another set of tests was carried out. Each motion condition of the wind tests (SIW) of Tables A1-A3 was tested without wind and with fixed rotor (NOW). In the NOW tests, only inertia and weight forces were measured.

The experiment focused on the thrust force, because it is a driving load in FOWTs. The aerodynamic thrust force was obtained according to this procedure, which is based on the assumption that the structural loads depend only on the type of motion and are the same in the NOW and SIW tests:

1. for any given motion condition, the SIW time histories are synchronized with the corresponding NOW. The reference signal for the procedure is the LVDT position;
2. SIW and NOW time histories are trimmed, keeping the maximum number of full periods of motion;
3. the aerodynamic forces are obtained subtracting the NOW time series from the SIW time series:

$$F_{a,i}(t) = F_{SIW,i}(t) - F_{NOW,i}(t) \qquad i = 1, \ldots, 6\,. \tag{5}$$

The procedure strongly relies on the assumption that the tower and blades behave as rigid bodies. This is in general true around the frequency of the imposed surge motion, which was in any case lower than the natural frequencies of the wind turbine components and, in particular, of the first tower fore-aft mode (6.5 Hz). For higher frequencies, the dynamic amplification associated with tower flexibility cannot be neglected anymore, and the results obtained based on the inertia-subtraction procedure are not reliable. In Mancini et al. (2020), an alternative inertia-subtraction algorithm is proposed to better deal with tower flexibility.

https://doi.org/10.5194/wes-2021-12
Preprint. Discussion started: 5 March 2021

eawe european academy of wind energy
Open Access WIND ENERGY SCIENCE DISCUSSIONS

4.4 Hot-wire wake measurements

An automatic traversing system was used to measure the three-component velocity in the wake of the wind turbine. The system, visible in Figure 7, consists of a moving arm mounting two hot-wire probes. Measurements were carried out with the traversing system spanning across the Y-Z plane (cross-wind, CW) or across the X-Z plane (along-wind, AW).

In the CW case, the measurement plane was 2.3D (5.48 m) downwind the wind turbine; this was the furthest distance given the size of the test chamber and it is considered to be part of the near-wake region Vermeer et al. (2003). One of the probe was mounted at hub-height, the other 0.2 m below. The probes were moved in the cross-wind direction, ranging from -1.6 m to 1.6 m with respect to the hub position, with a distance of 0.1 m between subsequent points. CW measurements were carried out both for the Rated2 and Above conditions, with and without surge motion.

In the AW case, the probes were mounted at hub-height, one next to the other: the first at y = 0.7 m, the second at y = 0.9 m. The probes were moved in the along-wind direction, ranging from 2.18 m to 5.48 m downwind the hub location, with a distance of 0.33 m between subsequent points. AW measurements were carried out only for the Rated2 condition, with and without surge motion.

Figure 7. Test setup for along-wind (AW) hot-wire measurements (left) and PIV (right) measurements.

4.5 PIV wake measurements

A PIV system was used to investigate a portion of the X-Z plane in the near-wake region. The PIV system encompasses an Nd:YAG double pulsed laser and two adjacent cameras, mounted on a traversing system, with a line of sight perpendicular to

https://doi.org/10.5194/wes-2021-12
Preprint. Discussion started: 5 March 2021

eawe european academy of wind energy
Open Access WIND ENERGY SCIENCE DISCUSSIONS

the laser sheet. The measurement area ranged from 0.6 m to 1.35 m downwind the hub location, and from 0.6 m to 1.39 m from the hub in the vertical direction. The image pairs were post-processed using PIVTEC PIVview 3C. PIV measurements were carried out for the Rated2 condition, with and without surge motion.

For the tests without surge motion, measurements were phase-locked to the blade-1 azimuth position (ψ). 100 image pairs were acquired for each measurement, from $\psi = 0°$ to $\psi = 120°$ with a $15°$ step, and from from $\psi = 120°$ to $\psi = 360°$ with a $30°$ step.

For the tests with surge motion, only the motion conditions with a frequency which is an integer sub-multiple of the rotor frequency (i.e. 4 Hz) were considered. Measurements were phase-locked to the surge position, and image pairs were acquired in several points of the motion cycle. Being the rotor frequency an integer multiple of the surge frequency, the blade-1 azimuth position is the same for all the measurements in a given surge position.

5 Key findings of the full-turbine experiments

5.1 Rotor thrust force

The analysis of the thrust force is based on a simplified description of the wind turbine rotor, that focus on the integral forces rather than considering the single blades. The rotor produces a thrust force:

$$T = \frac{1}{2}\rho\pi R^2 C_T V^2 , \tag{6}$$

where ρ is the air density, R the rotor radius, C_T the thrust coefficient and V the undisturbed wind speed. The thrust coefficient is set by the wind turbine operating condition, which is defined by the TSR λ and the collective pitch angle β:

$$C_T = C_T(\lambda, \beta), \qquad \lambda = \frac{\omega R}{V} . \tag{7}$$

The thrust force can be linearized based on a first-order Taylor expansion:

$$T \simeq T_0 + K_{VT}\Delta V + K_{\beta T}\Delta\beta + K_{\omega T}\Delta\omega , \tag{8}$$

where T_0 is the steady-state thrust force; ΔV, $\Delta\beta$ and $\Delta\omega$ are the variation of rotor speed, collective pitch angle and wind speed from their respective steady-state value; K_{VT}, $K_{\beta T}$ and $K_{\omega T}$ are the partial derivatives of thrust with respect to wind speed, collective pitch and rotor speed Bianchi et al. (2007). In the present case, collective pitch and rotor speed are fixed, so:

$$T \simeq T_0 + K_{VT}\Delta V , \tag{9}$$

with:

$$K_{VT} = \frac{T_0}{V}\left(2 - \frac{\partial C_T}{\partial\lambda}\bigg|_0 \frac{\lambda_0}{C_{T,0}}\right), \tag{10}$$

where λ_0 is the steady-state TSR and $C_{T,0}$ the steady-state thrust coefficient.

https://doi.org/10.5194/wes-2021-12
Preprint. Discussion started: 5 March 2021

eawe european academy of wind energy
Open Access WIND ENERGY SCIENCE DISCUSSIONS

The wind speed seen by any point of the rotor when the flow is smooth and the wind turbine moves in the surge direction is:

$$V = V_0 - \dot{x}, \qquad \Delta V = -\dot{x}\,, \tag{11}$$

where V_0 is the mean wind speed.

The thrust force is

$$T \simeq T_0 - K_{VT}\dot{x}, \qquad \Delta T = -K_{VT}\dot{x}\,. \tag{12}$$

The thrust force variation induced by the surge motion is predicted based only on the wind turbine steady-state operational data. Equation 12 is therefore herein referred to as quasi-steady theory. According to quasi-steady theory (QST), the thrust force variation depends only on the surge velocity.

The focus of the experimental force measurements is the surge-frequency thrust force. At the surge frequency, the effects of tower flexibility are small, and the thrust force is extracted from the tower-top force measurements based on the inertia-subtraction procedure presented in Section 4.3. The surge-frequency thrust force is:

$$\Delta T = |\Delta T| e^{j\phi}\,, \tag{13}$$

where $|\Delta T|$ is the amplitude of the thrust force at the surge frequency and ϕ is the phase with respect to the surge displacement. In general, the surge-frequency thrust force has a component in opposition of phase to the surge velocity, and one in opposition of phase to the surge acceleration. According to the QST model of Equation 12, the thrust force is perfectly in aligned to the surge velocity.

The adherence of the thrust force measurements to the QST model is studied based on the unsteady thrust force coefficient:

$$C_{\Delta T} = \frac{\Delta T}{\frac{1}{2}\rho\pi R^2 V^2}\,. \tag{14}$$

This non-dimensional representation is useful to make the outcomes of the experiment comparable to other studies. According to QST:

$$|\Delta T| = 2\pi f_s A_s K_{VT}\,, \tag{15}$$

and the unsteady thrust coefficient is:

$$C_{\Delta T}^{QST} = 2\pi f_r A_r C_0^*\,, \tag{16}$$

where $f_r = 1/V^*$ is the reduced surge-frequency, $A_r = A_s/D$ the reduced surge-amplitude, and:

$$C_0^* = \left(C_{T0}\left(2 - \frac{\partial C_T}{\partial \lambda}\bigg|_0 \frac{\lambda_0}{C_{T0}}\right)\right). \tag{17}$$

The unsteady thrust coefficient for the motion conditions investigated in the experiment is shown on the left of Figure 8. In the figure $C_{\Delta T}$ is divided by A_r and is reported as function of f_r. In this plot, the QST prediction corresponds to a straight

https://doi.org/10.5194/wes-2021-12
Preprint. Discussion started: 5 March 2021

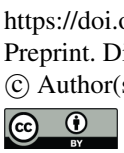

eawe european academy of wind energy
Open Access WIND ENERGY SCIENCE DISCUSSIONS

line, which slope is set by the wind turbine operating condition and the steady-state thrust characteristic. The dashed lines are obtained as in Equation 16 based on steady-state thrust coefficient of the wind turbine scale model Belloli et al. (2020). The phase of the thrust force is shown on the right of Figure 8. According to QST, the phase is -90°, regardless of the motion condition. For low values of f_r the thrust force measurements follow the QST. For increasing values of f_r, the thrust force has a small component in phase with the surge position, which is not predicted by QST. This is visualized by the phase ϕ, which increases above -90°, and by $C_{\Delta T}$, which shifts away from the QST line. A trend appears in $C_{\Delta T}$, but it is less evident in the phase ϕ, which is scattered in a range of $\pm 10°$ around -90°. This uncertainty is related to the fact that part of the thrust force opposed to the surge acceleration is in any case very small, and difficult to measure.

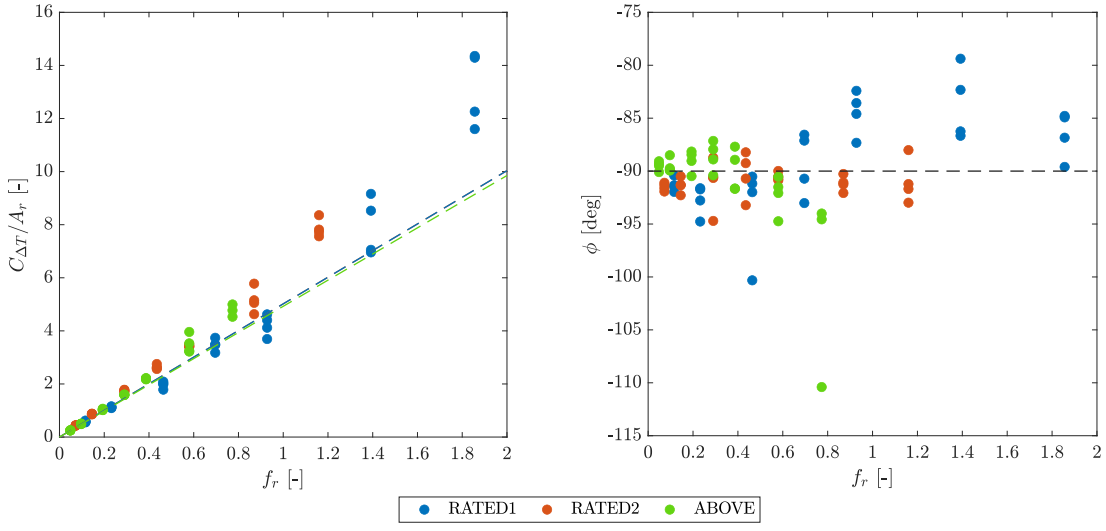

Figure 8. Left: unsteady thrust coefficient against reduced frequency; right: phase of the thrust force with respect to the surge motion against reduced frequency. RATED1 (blue), RATED2 (orange), ABOVE (green), quasi-steady theory (dashed lines).

5.2 Hot-wire wake measurements

The wake shape at hub-height is captured by the mean velocity deficit. The deficit for all the conditions that were investigated with hot-wire measurements is shown in Figure 9. The reduction of axial velocity is always higher in RATED2, where the wind turbine is operated at the maximum power coefficient, compared to ABOVE. The wake is also slightly asymmetric with respect to the hub. For any condition the velocity deficit is larger on the left side compared to the right. When the wind turbine moves, the wake is slightly narrower, meaning there is more energy in its outer region. Outside the boundaries of the rotor, a certain speed up is observable, which is caused by the wind tunnel blockage. Concerning the surge motion, it appears evident that it does not significantly change the mean wake deficit. Even if there are some major differences in the experiment (a porous disk was used to emulate the wind turbine rotor, measurements were carried out at a distance of 4.6D, the inflow was turbulent), this

https://doi.org/10.5194/wes-2021-12
Preprint. Discussion started: 5 March 2021

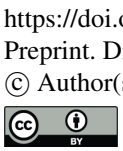

eawe european academy of wind energy
Open Access WIND ENERGY SCIENCE DISCUSSIONS

is in agreement with Schliffke et al. (2020), where it is evidenced that the surge motion does not affect the shape of the vertical wake profile.

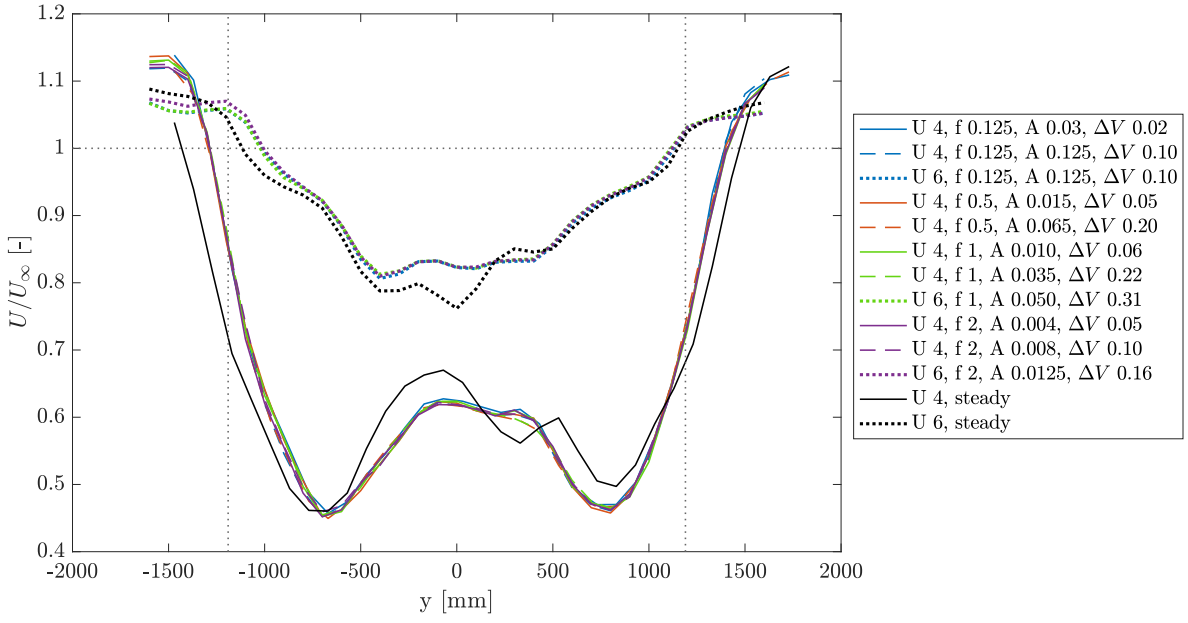

Figure 9. Mean velocity deficit at hub-height ($y = 0$ corresponds to the hub location, the rotor edge is marked by the vertical dotted lines) for the steady cases (i.e. without surge motion) and unsteady cases.

The frequency content of the wake at hub-height is studied plotting the PSD of the three velocity components measured in different points across the rotor. Figure 10 compares the spectral plots for the RATED2 case without and with surge motion, in particular with reference to the case of $f = 1\ Hz$, $A = 0.035\ m$. The energy content is concentrated in the outer region of the rotor and it is reasonably related to the blade-tip vortex. This distribution of energy is common also to any other RATED2 case. The asymmetry seen in the velocity deficit is found also in the spectra, and it is particularly evident in the vertical component W, which is associated with the rotor angular speed. Looking at the unsteady case, a strong harmonic component is visible at the frequency of motion, which is absent in the steady case. The surge-frequency harmonic is more evident in the axial velocity, compared to the other two velocity components. Another strong harmonic component is visible close to $f = 4\ Hz$, the 1P frequency, and it is associated with a slightly different pitch angle setting for the three blades.

The same analysis is carried out in Figure 11 for what concerns the ABOVE condition. In this case, energy is concentrated in the inner region of the rotor, witnessing the presence of a strong blade-root vortex. Also in this case, the 1P component is visible, at $f = 4.417\ Hz$ and the wake is slightly asymmetric. In the case with surge motion, an harmonic becomes evident at the surge frequency. The harmonic is equally present in the three velocity components.

https://doi.org/10.5194/wes-2021-12
Preprint. Discussion started: 5 March 2021

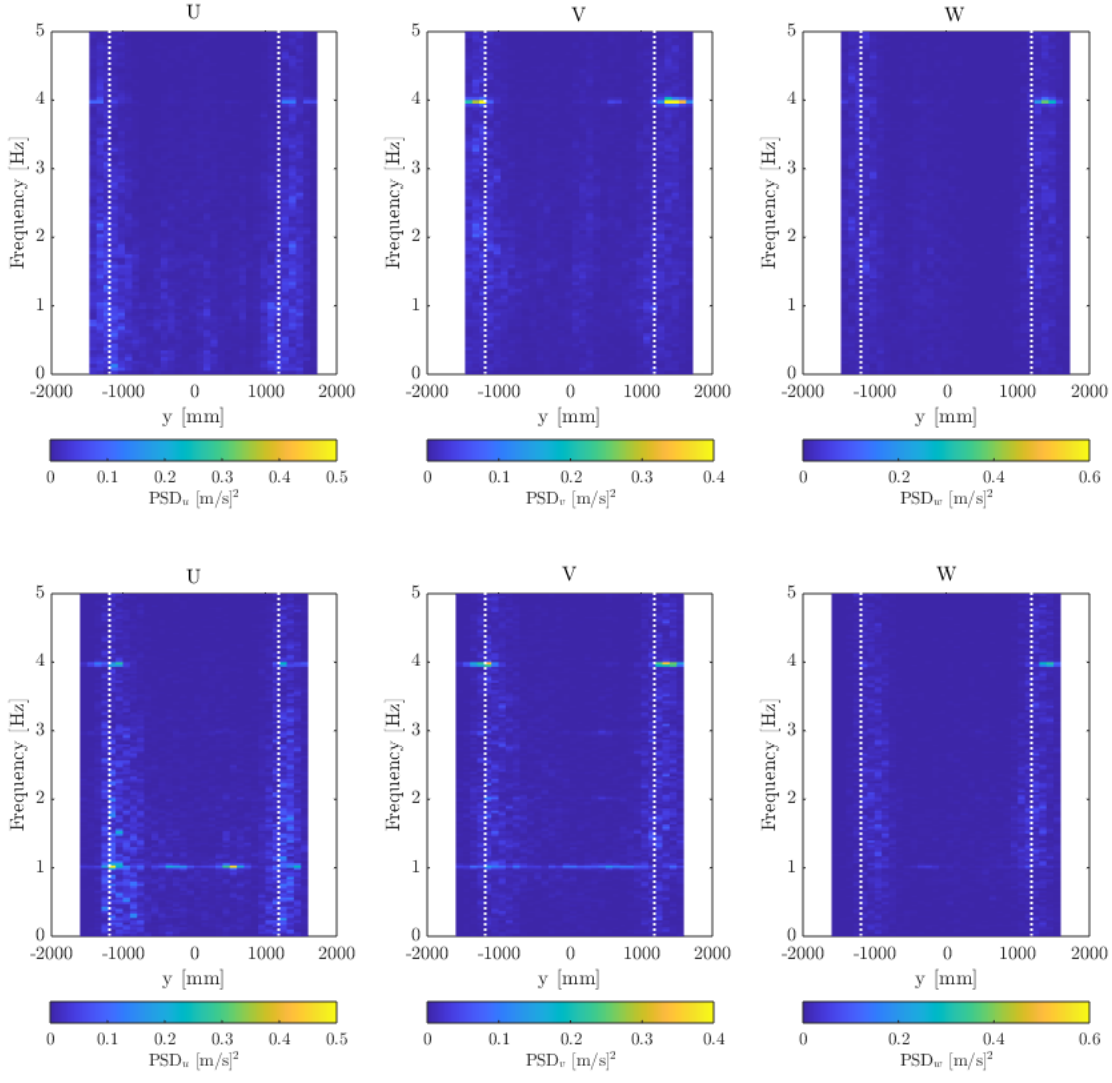

Figure 10. PSD of the hub-height wake velocity components (U axial, V lateral, W vertical) in different cross-wind positions ($y = 0$ corresponds to the hub location, the rotor edge is marked by the vertical dotted lines) for the RATED2 case. Top: steady condition; bottom: unsteady condition with $f = 1\ Hz$, $A = 0.035\ m$.

It is possible to have a more detailed description of the effect of the surge motion on the wake looking at two PSD functions. The analysis is carried out for the axial velocity component, since it is aligned with the surge direction and it is most affected by the wind turbine motion. The space-averaged PSD gives a description of the energy distribution in frequency and it is obtained

https://doi.org/10.5194/wes-2021-12
Preprint. Discussion started: 5 March 2021

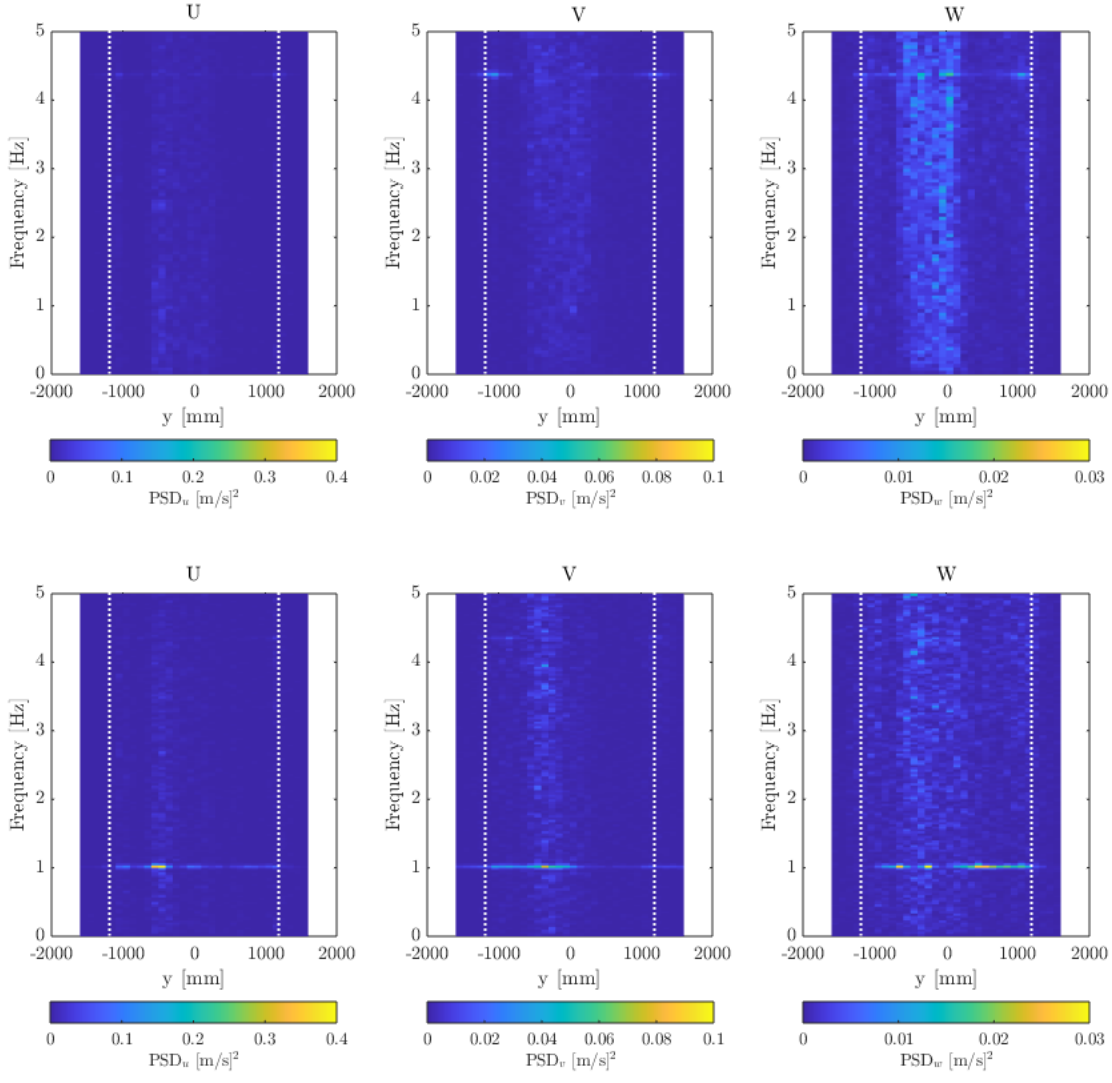

Figure 11. PSD of the hub-height wake velocity components (U axial, V lateral, W vertical) in different cross-wind positions ($y = 0$ corresponds to the hub location, the rotor edge is marked by the vertical dotted lines) for the ABOVE case. Top: steady condition; bottom: unsteady condition with $f = 1\ Hz$, $A = 0.05\ m$.

summing the PSD for all the measurement points:

$$\overline{U}_f = \frac{\sum_{y=1}^{n_y} U_{y,f}}{\sum_{y=1}^{n_y}\sum_{f=1}^{n_f} U^0_{y,f}}, \tag{18}$$

where $U_{y,f}$ is the PSD of the axial velocity at point y evaluated at frequency f, n_y is the number of points where the wake speed is measured, and n_f the number of discrete frequencies where the PSD is computed. $U^0_{y,f}$ denotes the PSD for the

https://doi.org/10.5194/wes-2021-12
Preprint. Discussion started: 5 March 2021

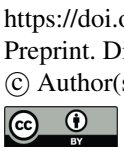

eawe european academy of wind energy
Open Access WIND ENERGY SCIENCE DISCUSSIONS

steady case with the same mean wind speed of $U_{y,f}$. This choice, allows to understand how the wake energy content changes because of the surge motion. The space-averaged PSD $\overline{U}_f$ for the investigated conditions is shown in Figure 12. In the steady case, energy is evenly spread below 1 Hz, and decreases smoothly increasing frequency. A peak is always present at the 1P frequency. The energy is greater in RATED2 compared to ABOVE, and also the 1P peak for the above cases is much lower than for the RATED2 cases. The spectrum for any of the unsteady cases is similar to the spectrum of the corresponding steady case, except for a peak at the surge frequency: energy is transferred in the wake by the surge motion. Similar findings, but for the far-wake of a porous disk, are reported in Schliffke et al. (2020). Looking at the PSD of Figure 12 it is also interesting to notice that, for a surge frequency up to 1 Hz, the amplitude of the surge-frequency peak is proportional to ΔV, but not linearly. The energy increment in the 2 Hz case is much lower than for any other motion condition with similar ΔV. The surge motion also amplifies the 1P harmonic and the amplification in RATED2 is much higher than in ABOVE conditions.

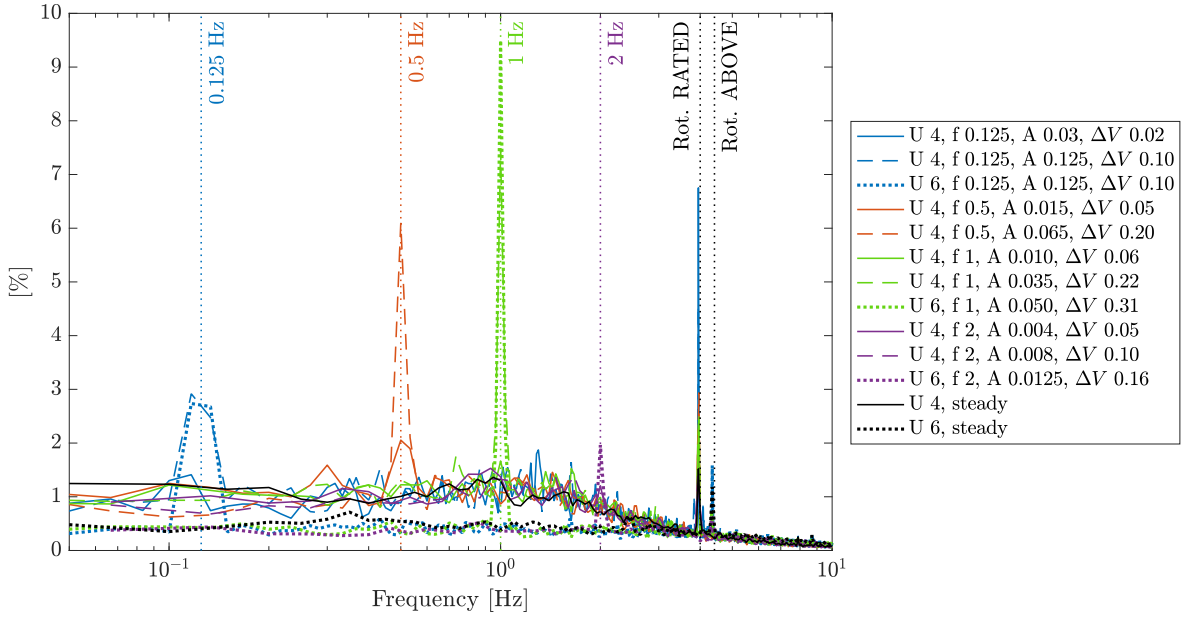

Figure 12. Space-averaged PSD of the hub-height axial velocity for different frequencies. The vertical dotted lines mark the frequencies of surge motion and the rotor frequency. In the legend: U is the mean wind speed, f the surge frequency, A the surge amplitude, ΔV the maximum surge velocity.

The frequency-averaged PSD defines how energy is distributed across the rotor and it is computed, for any measurement point, as the frequency-integral of the corresponding PSD:

$$\overline{U}_y = \frac{\sum_{f=1}^{n_f} U_{y,f}}{\sum_{y=1}^{n_y} \sum_{f=1}^{n_f} U_{y,f}} . \tag{19}$$

https://doi.org/10.5194/wes-2021-12
Preprint. Discussion started: 5 March 2021

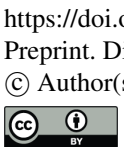

eawe european academy of wind energy
Open Access WIND ENERGY SCIENCE DISCUSSIONS

In this case, $U_{y,f}$ is used for normalization. The frequency-averaged PSDs $\overline{U}_y$ are reported in Figure 13. The energy space distribution is not affected by the type of motion, and it is strictly characteristic of the operating condition. In RATED2 conditions, energy is concentrated in the outer region of the rotor and it is associated with the blade-tip vortex. In ABOVE conditions, most of the energy is in the central part of the rotor, where the blade-root vortex is, whereas the contribution of the tip vortex is lower. More energy is present on the left than on the right of the hub and this is particularly evident in the ABOVE cases. The fact the shape of $\overline{U}_y$ remains the same, suggests the surge motion adds energy evenly across the rotor. In detail, it increases the axial travel velocity of vortices.

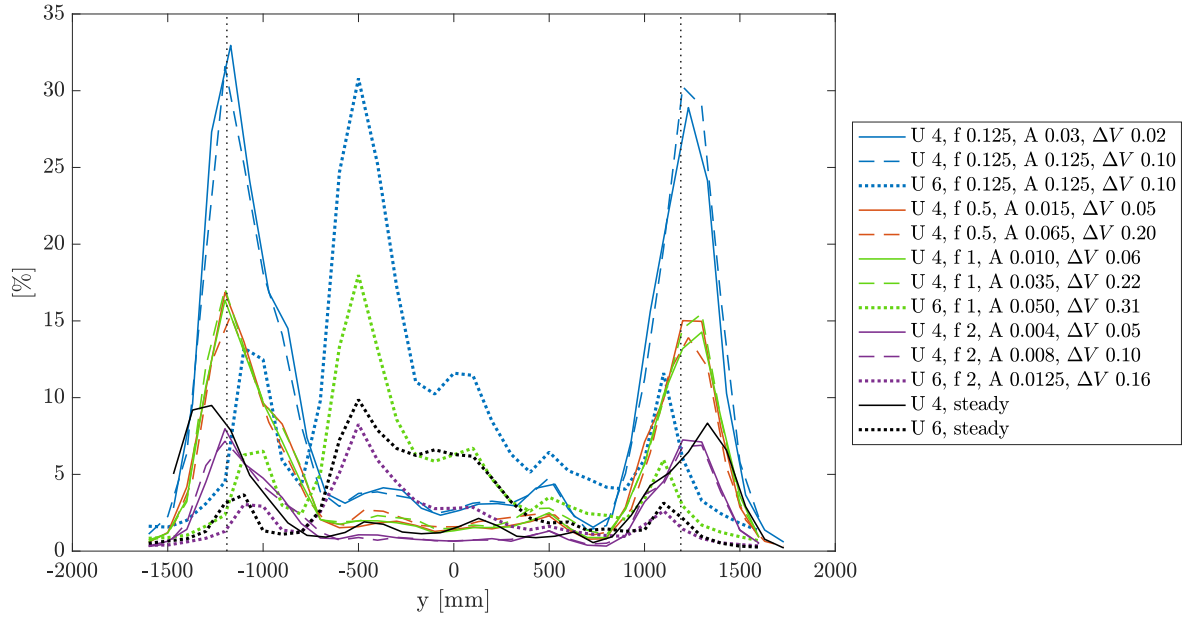

Figure 13. Frequency-averaged PSD of the hub-height axial velocity in different cross-wind positions ($y = 0$ corresponds to the hub location, the rotor edge is marked by the vertical dotted lines). In the legend: U is the mean wind speed, f the surge frequency, A the surge amplitude, ΔV the maximum surge velocity.

5.3 PIV wake measurements

PIV combined with a realistic wind turbine scale model, makes it possible to appreciate the structure of the wind turbine wake and investigate how it is affected by the surge motion. The focus is on the blade-tip vortex as it holds most of the wake energy. The blade-tip vortex is visualized by means of the magnitude of the vorticity, obtained from the in-plane velocity components (u, v).

Figure 14 reports the vorticity magnitude for the portion of the investigation area that contains the blade-tip vortex. The flow field was measured in RATED2 conditions without surge motion with a blade-1 azimuth of zero degrees. The tip-vortices shed

https://doi.org/10.5194/wes-2021-12
Preprint. Discussion started: 5 March 2021

eawe european academy of wind energy
Open Access WIND ENERGY SCIENCE DISCUSSIONS

by the blades are clearly seen. The vortices position does not change for subsequent PIV images captured in the same azimuthal position of blade-1.

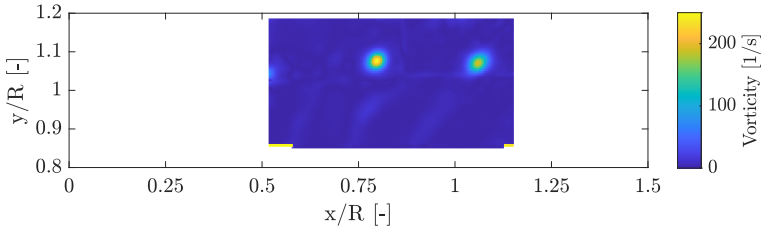

Figure 14. Vorticity for the RATED2 operating condition without surge motion. x/R and z/R are the axial and vertical distance from rotor rotor apex normalized by rotor radius. The origin of the axes is coincident with the rotor apex when the wind turbine is in the zero-surge position.

Figure 15 shows the vorticity magnitude in the same condition, but with a surge motion of frequency 1 Hz and amplitude 0.065 m. PIV images are acquired in eight different surge positions and a blade-1 azimuth of zero-degrees. The position of the tip-vortices is modified by the presence of the surge motion, and it varies periodically with the surge motion frequency. The mechanism behind the evolution of the wake is explained comparing two phases of the surge motion with equal but opposite velocity (e.g. phase 4 and phase 8 in Figure 15). When the rotor moves with a downwind velocity (phase 4), the tip vortices are released with a lower velocity than without surge motion and travel a lower distance in the wake; the opposite is true when the rotor moves with an upwind velocity (phase 8). This mechanism explains the increase of the surge-frequency energy content of the wake seen in hot-wire measurements. The behavior of the tip vortex was studied by means of CFD simulations in Cormier et al. (2018) with similar findings. Numerical simulations also show a stable vortex merging which is not evidenced by the experiment.

6 Conclusions

This paper presented the UNAFLOW experiments. Advanced wind tunnel measurements were carried out to improve knowledge about the unsteady aerodynamics of floating offshore wind turbines. Data were also produced to be a reference for the validation of numerical codes.

Thrust force plays a crucial role in floating wind turbine, as it drives the dynamic response of the platform surge and pitch modes. The thrust force was investigated by means tower-top force measurements. The thrust force measurement for several surge-motion conditions is compared to the prediction of quasi-steady theory with good agreement up to a reduced frequency of 0.5. Above this frequency, unsteady effects may be present. However, it is difficult to quantify the unsteady component of the thrust force by means of experiments. Its measurement is uncertain as it represents just a small fraction of the total rotor force.

https://doi.org/10.5194/wes-2021-12
Preprint. Discussion started: 5 March 2021

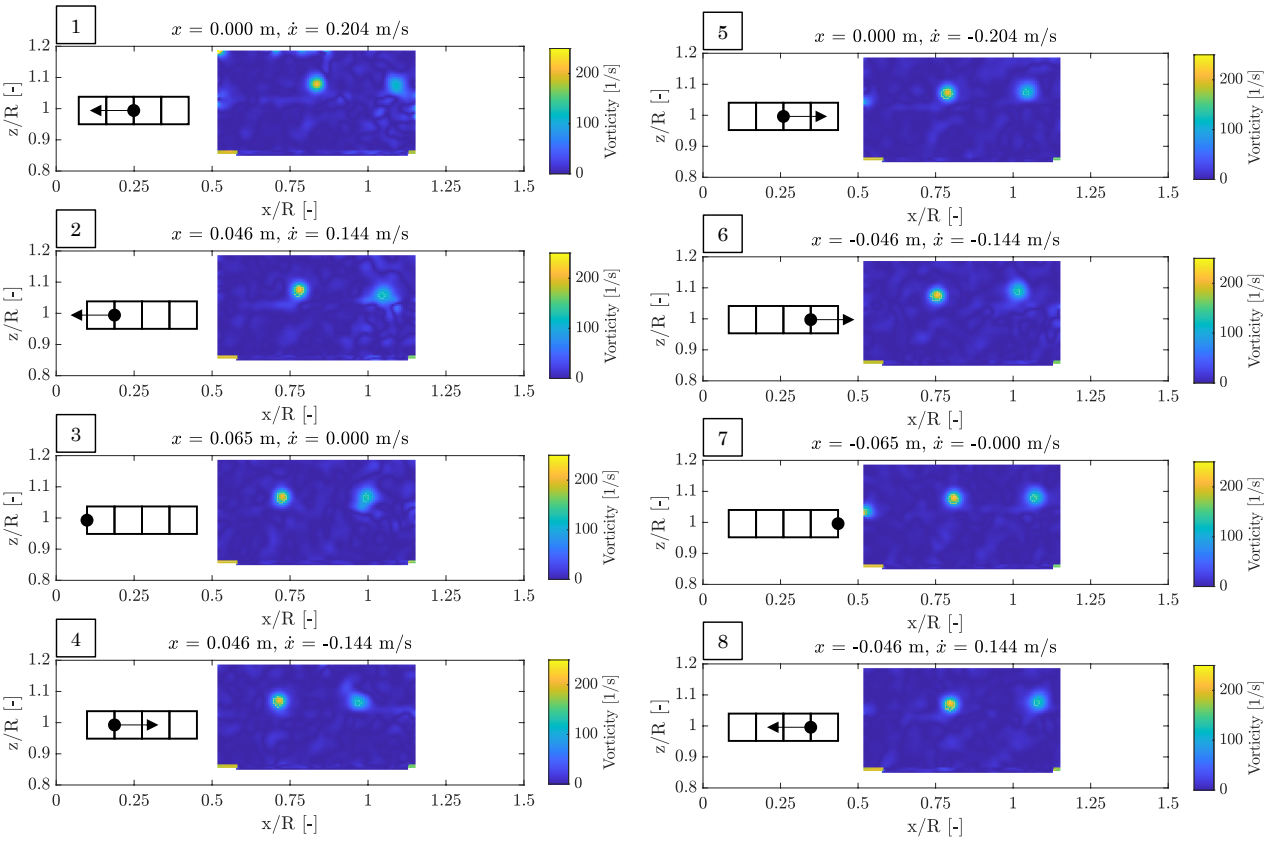

Figure 15. Vorticity for eight subsequent wind turbine positions in a surge cycle of frequency 0.5 Hz and amplitude 0.065 m and RATED2 conditions. The blade-1 azimuth is always zero degrees. x/R and z/R are the axial and vertical distance from rotor rotor apex normalized by rotor radius. The origin of the axes is coincident with the rotor apex when the wind turbine is in the zero-surge position.

Hub-height hot-wire anemometry and PIV surveys were carried out to investigate how the wake of the wind turbine is affected by the surge motion. Hot-wire measurements show that the mean hub-height velocity deficit with surge motion is the same as with still wind turbine. On the other side, the spectral content of the wake clearly shows the trace of the imposed surge motion. In particular, the surge motion adds energy to the wake, and the energy increment is proportional to the maximum surge velocity. PIV measurements, which are phase-locked to the wind turbine position in the surge cycle and to the rotor azimuth, show that the surge motion modifies the travel speed of the blade-tip vortex, that varies periodically at the frequency of the surge motion.

The experiment highlighted some research questions that are still opened and could be answered with further investigations. In detail:

https://doi.org/10.5194/wes-2021-12
Preprint. Discussion started: 5 March 2021

- the coupled dynamics of rotor and platform rigid-body motions is crucial for the control of floating wind turbines. Because of this coupled dynamics, closed-loop pitch-to-feather control strategies may lead to an unstable response of the system Larsen and Hanson (2007); Jonkman (2008); van der Veen et al. (2012). One plausible solution is to design the controller based on a reduced-order model of the FOWT Lemmer (ne Sandner). In state-of-the-art control-design models, the rotor aerodynamics is often introduced by means of quasi-steady theory Fontanella et al. (2020); Lemmer et al. (2020). In order to improve the current control practice, it would be useful to develop a control-oriented model of the unsteady thrust force. Experimental data would be useful to calibrate and validate such a model.

- the platform pitch mode is very sensitive to the interaction with rotor, and a correct description of this phenomenon is essential in model-based wind turbine control strategies. Moreover, numerical simulations have shown that pitch motion has a strong influence on the vertical wake deflection Wise and Bachynski (2020), which has the potential to be exploited for farm control purposes. The pitch shares some similarities with the surge mode, as it causes an along-wind motion of the rotor. However, in the surge case, the wind speed variation across the rotor is uniform, whereas in the pitch case, the flow seen by the rotor is skewed. It may be worth carrying out experiments for the pitch motion;

- unsteady aerodynamic effects appear to be more relevant at the higher reduced frequencies. It would be interesting to investigate surge-frequencies higher than those considered in this experiment. This is in general complex because of the risk of exciting the flexible modes of the wind turbine scale model. A potential solution is represented by numerical experiments. Numerical models could be validated based on the experimental data that are already available, and then used to study the other conditions, which may be unpractical to explore with experiments;

- the interaction between surge motion and wind turbine wake deserves further attention. A better understanding of the wake inflow may help explaining the unsteady behavior of the rotor thrust force. Moreover, it would lead to improved engineering wake models, which are needed for the design and optimization of future floating wind farms.

Data availability. All the data of the UNAFLOW experiment, from 2D and full-turbine tests, stored in the ftp ftp (2018). Credentials for the access are available upon request to the authors.

https://doi.org/10.5194/wes-2021-12
Preprint. Discussion started: 5 March 2021

eawe european academy of wind energy
Open Access WIND ENERGY SCIENCE DISCUSSIONS

Appendix A: Test matrices

Table A1. RATED1 test matrix (RS is the rotor speed, β is the rotor collective pitch angle). The CW, AW, PIV columns indicates wether if a cross-wind, along-wind or PIV measurement of the wake was carried out.

V [m/s]	f_s [Hz]	A_s [m]	V_w^* [-]	TSR [-]	RS [rpm]	β [deg]	CW	AW	PIV
2.5	0.125	0.125	8.62	7.5	150	0			
2.5	0.125	0.120	8.62	7.5	150	0			
2.5	0.125	0.080	8.62	7.5	150	0			
2.5	0.125	0.040	8.62	7.5	150	0			
2.5	0.250	0.080	4.31	7.5	150	0			
2.5	0.250	0.060	4.31	7.5	150	0			
2.5	0.250	0.040	4.31	7.5	150	0			
2.5	0.250	0.020	4.31	7.5	150	0			
2.5	0.500	0.040	2.16	7.5	150	0			
2.5	0.500	0.030	2.16	7.5	150	0			
2.5	0.500	0.020	2.16	7.5	150	0			
2.5	0.500	0.010	2.16	7.5	150	0			
2.5	0.750	0.030	1.44	7.5	150	0			
2.5	0.750	0.020	1.44	7.5	150	0			
2.5	0.750	0.015	1.44	7.5	150	0			
2.5	0.750	0.007	1.44	7.5	150	0			
2.5	1.000	0.030	1.08	7.5	150	0			
2.5	1.000	0.025	1.08	7.5	150	0			
2.5	1.000	0.015	1.08	7.5	150	0			
2.5	1.000	0.008	1.08	7.5	150	0			
2.5	1.500	0.015	0.72	7.5	150	0			
2.5	1.500	0.010	0.72	7.5	150	0			
2.5	1.500	0.007	0.72	7.5	150	0			
2.5	1.500	0.0035	0.72	7.5	150	0			
2.5	2.000	0.010	0.54	7.5	150	0			
2.5	2.000	0.007	0.54	7.5	150	0			
2.5	2.000	0.005	0.54	7.5	150	0			
2.5	2.000	0.0025	0.54	7.5	150	0			

https://doi.org/10.5194/wes-2021-12
Preprint. Discussion started: 5 March 2021

eawe european academy of wind energy
Open Access WIND ENERGY SCIENCE DISCUSSIONS

Table A2. RATED2 test matrix (RS is the rotor speed, β is the rotor collective pitch angle). The CW, AW, PIV columns indicates wether if a cross-wind, along-wind or PIV measurement of the wake was carried out.

V [m/s]	f_s [Hz]	A_s [m]	V_w^* [-]	TSR [-]	RS [rpm]	β [deg]	CW	AW	PIV
4.0	0.125	0.125	13.79	7.5	241	0	×	×	×
4.0	0.125	0.100	13.79	7.5	241	0			
4.0	0.125	0.065	13.79	7.5	241	0			
4.0	0.125	0.030	13.79	7.5	241	0	×		×
4.0	0.250	0.125	6.90	7.5	241	0			
4.0	0.250	0.100	6.90	7.5	241	0			
4.0	0.250	0.065	6.90	7.5	241	0			
4.0	0.250	0.030	6.90	7.5	241	0			
4.0	0.500	0.065	3.45	7.5	241	0	×	×	×
4.0	0.500	0.050	3.45	7.5	241	0			
4.0	0.500	0.035	3.45	7.5	241	0			
4.0	0.500	0.015	3.45	7.5	241	0	×		×
4.0	0.750	0.040	2.30	7.5	241	0			
4.0	0.750	0.030	2.30	7.5	241	0			
4.0	0.750	0.020	1.44	7.5	241	0			
4.0	0.750	0.010	1.44	7.5	241	0			
4.0	1.000	0.050	1.72	7.5	241	0			
4.0	1.000	0.035	1.72	7.5	241	0	×	×	×
4.0	1.000	0.025	1.72	7.5	241	0			
4.0	1.000	0.010	1.72	7.5	241	0	×		×
4.0	1.500	0.020	1.15	7.5	241	0			
4.0	1.500	0.015	1.15	7.5	241	0			
4.0	1.500	0.010	1.15	7.5	241	0			
4.0	1.500	0.005	1.15	7.5	241	0			
4.0	2.000	0.015	0.86	7.5	241	0			
4.0	2.000	0.0125	0.86	7.5	241	0			
4.0	2.000	0.008	0.86	7.5	241	0	×	×	×
4.0	2.000	0.004	0.86	7.5	241	0	×		×

https://doi.org/10.5194/wes-2021-12
Preprint. Discussion started: 5 March 2021

eawe european academy of wind energy
Open Access WIND ENERGY SCIENCE DISCUSSIONS

Table A3. ABOVE test matrix (RS is the rotor speed, β is the rotor collective pitch angle). The CW, AW, PIV columns indicates wether if a cross-wind, along-wind or PIV measurement of the wake was carried out.

V [m/s]	f_s [Hz]	A_s [m]	V_w^* [-]	TSR [-]	RS [rpm]	β [deg]	CW	AW	PIV
6.0	0.125	0.125	20.69	5.5	265	12.5			
6.0	0.125	0.100	20.69	5.5	265	12.5			
6.0	0.125	0.065	20.69	5.5	265	12.5			
6.0	0.125	0.030	20.69	5.5	265	12.5			
6.0	0.250	0.125	10.34	5.5	265	12.5			
6.0	0.250	0.100	10.34	5.5	265	12.5			
6.0	0.250	0.065	10.34	5.5	265	12.5			
6.0	0.250	0.030	10.34	5.5	265	12.5			
6.0	0.500	0.100	5.17	5.5	265	12.5			
6.0	0.500	0.075	5.17	5.5	265	12.5			
6.0	0.500	0.050	5.17	5.5	265	12.5			
6.0	0.500	0.025	5.17	5.5	265	12.5			
6.0	0.750	0.065	3.45	5.5	265	12.5			
6.0	0.750	0.050	3.45	5.5	265	12.5			
6.0	0.750	0.030	1.44	5.5	265	12.5			
6.0	0.750	0.015	1.44	5.5	265	12.5			
6.0	1.000	0.070	2.59	5.5	265	12.5			
6.0	1.000	0.050	2.59	5.5	265	12.5			
6.0	1.000	0.035	2.59	5.5	265	12.5			
6.0	1.000	0.018	2.59	5.5	265	12.5			
6.0	1.500	0.030	1.72	5.5	265	12.5			
6.0	1.500	0.025	1.72	5.5	265	12.5			
6.0	1.500	0.015	1.72	5.5	265	12.5			
6.0	1.500	0.008	1.72	5.5	265	12.5			
6.0	2.000	0.018	1.29	5.5	265	12.5	×		
6.0	2.000	0.0125	1.29	5.5	265	12.5	×		
6.0	2.000	0.006	1.29	5.5	265	12.5	×		

https://doi.org/10.5194/wes-2021-12
Preprint. Discussion started: 5 March 2021

eawe european academy of wind energy
Open Access WIND ENERGY SCIENCE DISCUSSIONS

Author contributions. AF revised the experimental dataset helping to get the most recent results. IB was responsible of the full-turbine experiments and helped define the experimental methodology. RM carried out the 2D experiments and processed the respective data. MB and AZ supervised and promoted the research activity. Finally, AF prepared the manuscript of this article with contribution from all co-authors.

Competing interests. The authors declare that they have no conflict of interest.

https://doi.org/10.5194/wes-2021-12
Preprint. Discussion started: 5 March 2021

eawe european academy of wind energy
Open Access WIND ENERGY SCIENCE DISCUSSIONS

References

Wind/Wave Basin Verification of a Performance-Matched Scale-Model Wind Turbine on a Floating Offshore Wind Turbine Platform, vol. Volume 9B: Ocean Renewable Energy of *International Conference on Offshore Mechanics and Arctic Engineering*, https://doi.org/10.1115/OMAE2014-24166, https://doi.org/10.1115/OMAE2014-24166, 2014.

A Formulation for the Unsteady Aerodynamics of Floating Wind Turbines, With Focus on the Global System Dynamics, vol. Volume 10: Ocean Renewable Energy of *International Conference on Offshore Mechanics and Arctic Engineering*, https://doi.org/10.1115/OMAE2017-61925, https://doi.org/10.1115/OMAE2017-61925, v010T09A055, 2017.

UNAFLOW data repository, ftps://www.unaflow.mecc.polimi.it, 2018.

Galleria del Vento Politecnico di Milano, http://www.windtunnel.polimi.it, 2019.

Bak, C., Zahle, F., Bitsche, R., Taeseong, K., Yde, A., Henriksen, L. C., Hansen, M. H., Jose, J. P. A. A., Gaunaa, M., and Natarajan, A.: The DTU 10-MW Reference Wind Turbine, DTU Wind Energy Report, 2013.

Bayati, I., Belloli, M., Bernini, L., and Zasso, A.: Wind tunnel validation of AeroDyn within LIFES50+ project: imposed Surge and Pitch tests, Journal of Physics: Conference Series, 753, 092 001, https://doi.org/10.1088/1742-6596/753/9/092001, https://doi.org/10.1088/1742-6596/753/9/092001, 2016.

Bayati, I., Belloli, M., Bernini, L., Giberti, H., and Zasso, A.: Scale model technology for floating offshore wind turbines, IET Renewable Power Generation, 11, 1120–1126, https://doi.org/10.1049/iet-rpg.2016.0956, 2017.

Bayati, I., Belloli, M., Bernini, L., and Zasso, A.: Aerodynamic design methodology for wind tunnel tests of wind turbine rotors, Journal of Wind Engineering and Industrial Aerodynamics, 167, 217 – 227, https://doi.org/https://doi.org/10.1016/j.jweia.2017.05.004, http://www.sciencedirect.com/science/article/pii/S0167610517301368, 2017a.

Bayati, I., Belloli, M., Bernini, L., and Zasso, A.: Wind Tunnel Wake Measurements of Floating Offshore Wind Turbines, vol. 137, pp. 214–222, https://doi.org/10.1016/j.egypro.2017.10.375, https://www.scopus.com/inward/record.uri?eid=2-s2.0-85032015856&doi=10.1016%2fj.egypro.2017.10.375&partnerID=40&md5=aac148722a514dec153f833fee76b361, 2017b.

Belloli, M., Bayati, I., Facchinetti, A., Fontanella, A., Giberti, H., La Mura, F., Taruffi, F., and Zasso, A.: A hybrid methodology for wind tunnel testing of floating offshore wind turbines, Ocean Engineering, 210, https://doi.org/10.1016/j.oceaneng.2020.107592, https://www.scopus.com/inward/record.uri?eid=2-s2.0-85085751799&doi=10.1016%2fj.oceaneng.2020.107592&partnerID=40&md5=e3b5533c595a58bc2d7e7684dc63bb95, 2020.

Bianchi, F., de Battista, H., and Mantz, R.: Wind Turbine Control Systems, Springer, https://doi.org/10.1007/1-84628-493-7, 2007.

Boorsma, K. and Caboni, M.: Numerical analysis and validation of unsteady aerodynamics for floating offshore wind turbines, TNO 2020 R11345, 880224, http://resolver.tudelft.nl/uuid:10b69f85-dd5a-4f74-ac68-fdc62c01ead3, 2020.

Cormier, M., Caboni, M., Lutz, T., Boorsma, K., and Kramer, E.: Numerical analysis of unsteady aerodynamics of floating offshore wind turbines, Journal of Physics: Conference Series, 1037, 072 048, https://doi.org/10.1088/1742-6596/1037/7/072048, https://doi.org/10.1088%2F1742-6596%2F1037%2F7%2F072048, 2018.

de Vaal, J., Hansen, M., and Moan, T.: Effect of wind turbine surge motion on rotor thrust and induced velocity, Wind Energy, 17, 105–121, https://doi.org/https://doi.org/10.1002/we.1562, https://onlinelibrary.wiley.com/doi/abs/10.1002/we.1562, 2014.

Fontanella, A., Al, M., van der Hoek, D., Liu, Y., van Wingerden, J., and Belloli, M.: A control-oriented wave-excited linear model for offshore floating wind turbines, Journal of Physics: Conference Series, 1618, 022 038, https://doi.org/10.1088/1742-6596/1618/2/022038, https://doi.org/10.1088%2F1742-6596%2F1618%2F2%2F022038, 2020.

https://doi.org/10.5194/wes-2021-12
Preprint. Discussion started: 5 March 2021

Hu, H., Khosravi, M. M., and Sarkar, P.: An Experimental Investigation on the Performance and the Wake Characteristics of a Wind Turbine Subjected to Surge Motion, https://doi.org/10.2514/6.2015-1207, https://arc.aiaa.org/doi/abs/10.2514/6.2015-1207, 2015.

Jonkman, J.: Influence of Control on the Pitch Damping of a Floating Wind Turbine, https://doi.org/10.2514/6.2008-1306, https://arc.aiaa.org/doi/abs/10.2514/6.2008-1306, 2008.

Larsen, T. and Hanson, T.: A method to avoid negative damped low frequent tower vibrations for a floating, pitch controlled wind turbine, vol. 75, https://doi.org/10.1088/1742-6596/75/1/012073, https://www.scopus.com/inward/record.uri?eid=2-s2.0-34548156706&doi=10.1088%2f1742-6596%2f75%2f1%2f012073&partnerID=40&md5=da0d731b888cd0eaf76d9406fbe321d6, 2007.

Lemmer, F., Yu, W., Luhmann, B., Schlipf, D., and Cheng, P. W.: Multibody modeling for concept-level floating offshore wind turbine design, Multibody System Dynamics, 49, 203 – 236, https://doi.org/10.1007/s11044-020-09729-x, https://doi.org/10.1007/s11044-020-09729-x, 2020.

Lemmer (ne Sandner), F., Yu, W., Schlipf, D., and Cheng, P. W.: Robust gain scheduling baseline controller for floating offshore wind turbines, Wind Energy, 23, 17–30, https://doi.org/10.1002/we.2408, https://onlinelibrary.wiley.com/doi/abs/10.1002/we.2408, 2020.

Mancini, S., Boorsma, K., Caboni, M., Cormier, M., Lutz, T., Schito, P., and Zasso, A.: Characterization of the unsteady aerodynamic response of a floating offshore wind turbine, https://doi.org/10.5194/wes-2020-94, 2020.

R. Farrugia and T. Sant and D. Micallef: Investigating the aerodynamic performance of a model offshore floating wind turbine, Renewable Energy, 70, 24 – 30, https://doi.org/https://doi.org/10.1016/j.renene.2013.12.043, http://www.sciencedirect.com/science/article/pii/S0960148114000147, Special issue on aerodynamics of offshore wind energy systems and wakes, 2014.

Schliffke, B., Aubrun, S., and Conan, B.: Wind Tunnel Study of a "Floating" Wind Turbine's Wake in an Atmospheric Boundary Layer with Imposed Characteristic Surge Motion, Journal of Physics: Conference Series, 1618, 062 015, https://doi.org/10.1088/1742-6596/1618/6/062015, https://doi.org/10.1088%2F1742-6596%2F1618%2F6%2F062015, 2020.

Shifeng Fu and Yaqing Jin and Yuan Zheng and Leonardo P. Chamorro: Wake and power fluctuations of a model wind turbine subjected to pitch and roll oscillations, Applied Energy, 253, 113 605, https://doi.org/https://doi.org/10.1016/j.apenergy.2019.113605, http://www.sciencedirect.com/science/article/pii/S0306261919312796, 2019.

van der Veen, G., Couchman, I., and Bowyer, R.: Control of floating wind turbines, in: 2012 American Control Conference (ACC), pp. 3148–3153, https://doi.org/10.1109/ACC.2012.6315120, 2012.

Vermeer, L., Sazrensen, J., and Crespo, A.: Wind turbine wake aerodynamics, Progress in Aerospace Sciences, 39, 467 – 510, https://doi.org/https://doi.org/10.1016/S0376-0421(03)00078-2, http://www.sciencedirect.com/science/article/pii/S0376042103000782, 2003.

Wise, A. S. and Bachynski, E. E.: Wake meandering effects on floating wind turbines, Wind Energy, 23, 1266–1285, https://doi.org/10.1002/we.2485, https://onlinelibrary.wiley.com/doi/abs/10.1002/we.2485, 2020.